Crossover from Fermi to Bose polarons in one- and two-dimensional interacting Fermi gases

Yue-Ran Shi [1,2,3] Ruijin Liu,[4,*] and Wei Zhang [1,2,5,†]

[1]*Department of Physics and Beijing Key Laboratory of Opto-electronic Functional Materials and Micro-nano Devices, Renmin University of China, Beijing 100872, China*

[2]*Key Laboratory of Quantum State Construction and Manipulation (Ministry of Education), Renmin University of China, Beijing 100872,China*

[3]*Institute of Theoretical Physics, Chinese Academy of Sciences, Beijing 100190, China*

[4]*Institute of Theoretical Physics, University of Science and Technology Beijing, Beijing 100083, China*

[5]*Beijing Academy of Quantum Information Sciences, Beijing 100193, China*

(Received 26 February 2024; revised 10 June 2024; accepted 8 July 2024; published 25 July 2024)

We investigate the Fermi-polaron system with one mobile impurity immersed atop a two-component interacting fermion bath in one- and two-dimensional square lattices, where the impurity atom interacts with only one species (the spin-up component) of the background. The ground state with a given total momentum can be approximated by an extended Gaussian state, which is constructed from the combination of Gaussian states and a non-Gaussian polaronic transformation (Lee-Low-Pines transformation). In the few-body limit, the variational energies of two- and three-body systems show good agreement with exact results, which indicates the validity of the non-Gaussian variational method. We then move on to the many-body limit, i.e., the polaron problem with an interacting background. We choose two representative fillings of the background fermions, $\rho = 1/4, 1/2$, and obtain the corresponding ground states. Our results show that the system will undergo a smooth crossover from a Fermi-polaron to a Bose-polaron system as the interaction between background fermions increases. We further analyze the double occupancy and momentum distribution of the background fermions and find that the impurity will not significantly affect the background pairing.

DOI: 10.1103/PhysRevA.110.013324

I. INTRODUCTION

The fate of an impurity particle interacting with a medium is a key building block in the understanding of complex quantum many-body systems. One notable example is the concept of polarons originally proposed by Landau and Pekar [1], which is of great interest in the context of transport properties in semiconducting, superconducting, and insulating materials in condensed-matter physics [2,3]. Recently, the study of polarons has been extended to ultracold atomic gases, and polarons have been further classified as Bose polarons or Fermi polarons based on the statistical properties of composite particles in the background medium. Thanks to technological advances such as the Feshbach resonance and optical lattice, both Fermi and Bose polarons have been realized and studied extensively in experiments [4–14], in which the attractive and repulsive branches of polaron spectra have been explored [15,16]. From a theoretical aspect, a variety of methods have been used to reveal the nature of polarons, including the Feynman path-integral treatment [17–20], quantum Monte Carlo methods [21–26], the transition-matrix approach [27–29], and renormalization- group theory [30,31]. Variational methods based on the Chevy-like ansatz [32] and Gaussian states [33,34] are also used to describe polaron properties and investigate the existence of a transition to a molecule state. It has been suggested that a polaron-molecule transition exists in the Fermi-polaron system, while the Bose polaron undergoes a smooth crossover from a polaronic to a bound molecule state with increasing interspecies couplings. Also, a metastable repulsive polaron state is found in both the Fermi [27,35] and Bose [19,36,37] cases.

In addition to the rich polaronic physics, polarons may also serve as a sensitive probe of the properties of the background, especially for strongly interacting many-body systems [38,39]. For example, it is of great interest to consider the polaron problem in a two-component Fermi superfluid, which is one of the most notable quantum phenomena universally in condensed-matter physics [40], atomic physics [41–44], nuclear physics [45,46], and astrophysics [47]. With tuning of the intercomponent interaction, the background of a two-component gas undergoes a crossover from the weakly interacting BCS Fermi superfluid to a Bose-Einstein condensate (BEC) of paired molecules. It is expected that the immersed impurity will change from a Fermi polaron to a Bose polaron along the BCS-BEC crossover. A previous study suggested that the treatment based on BCS theory is valid only in the weakly interacting limit and the intermediate region, while in the strongly interacting regime the exact three-body effect must be taken into account [44]. Although the transition between the two limiting cases is expected, a unified theory

*Contact author: rjliu@ustb.edu.cn

†Contact author: wzhangl@ruc.edu.cn

of the crossover is still lacking. Thus, it is of interest to provide a consistent description of the entire Fermi-Bose-polaron crossover with trustable precision.

In this work, we implement a non-Gaussian variational method to study the ground state of an impurity particle immersed in a two-component Fermi gas with attractive interaction. For simplicity, the impurity is assumed to couple with only one species of fermions (spin ↑), such that analytic results are available in both the BCS and BEC limits. To make a connection with ultracold atomic gases in optical lattices, the background is described by an attractive Fermi Hubbard model under the single-band approximation, where the on-site interaction and intersite hopping can be rather freely adjusted by tuning optical lattice parameters and the Feshbach resonance. We separate the impurity degrees of freedom via the Lee-Low-Pines transformation [48] and use a trial state of Gaussian form to approximate the ground state of the interacting background. The variational parameters are then fixed by imaginary-time evolution, and the ground state is determined by performing an inverse Lee-Low-Pines transformation, which is in a non-Gaussian form in general. For both one- (1D) and two-dimensional (2D) square lattices with representative fillings $\rho = 1/4$ and $1/2$, we observe a smooth crossover from a Fermi-polaron state to a Bose-polaron state along with the BCS-BEC crossover of the background. The theoretical calculations can be witnessed by both the spectroscopic measurement of polaron energy [7,49,50] and the *in situ* imaging results of double occupancy [51]. This method can be easily expanded to spin- or mass-imbalanced systems by changing the chemical potential or hopping parameters. The calculation can also be extended to other kinds of lattice configurations in different dimensions without much numerical expense. Further, if one performs a real-time evolution to obtain the variational parameters, the method can be applied to study out-of-equilibrium dynamics.

The remainder of this paper is organized as follows. In Sec. II we formulate the general non-Gaussian variational method for the interacting polaron problem. In Sec. III, the ground-state energy is calculated for some limiting cases, where exact results can be obtained as a benchmark. Then we obtain the ground-state energy, double occupancy, and momentum distribution in 1D and 2D lattices with different fermion fillings to witness the Fermi-Bose-polaron crossover. In Sec. IV we summarize our results and discuss promising directions for future studies.

II. HAMILTONIAN AND NON-GAUSSIAN VARIATIONAL METHOD

We consider an attractive Hubbard model of spin-1/2 fermions in a D-dimensional square lattice with an impurity interacting with only the spin-↑ component, as illustrated in Fig. 1. The Hamiltonian is written as

$$\begin{aligned}\hat{H} =& -t_{\mathrm{f}} \sum_{\langle \mathbf{ij}\rangle,\sigma} c^{\dagger}_{\mathbf{i}\sigma} c_{\mathbf{j}\sigma} - t_{\mathrm{b}} \sum_{\langle \mathbf{ij}\rangle} b^{\dagger}_{\mathbf{i}} b_{\mathbf{j}} + U_{\mathrm{ff}} \sum_{\mathbf{i}} \hat{n}_{\mathbf{i}\uparrow}\hat{n}_{\mathbf{i}\downarrow} \\ &+ U_{\mathrm{bf}} \sum_{\mathbf{i}} c^{\dagger}_{\mathbf{i}\uparrow} c_{\mathbf{i}\uparrow} b^{\dagger}_{\mathbf{i}} b_{\mathbf{i}} - \sum_{\mathbf{i}\sigma} \mu_{\sigma} c^{\dagger}_{\mathbf{i}\sigma} c_{\mathbf{i}\sigma}, \end{aligned} \tag{1}$$

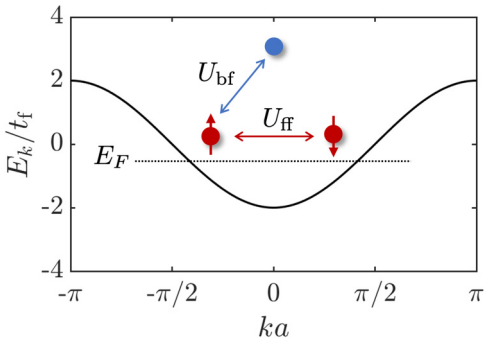

FIG. 1. Schematic plot of the 1D lattice energy dispersions $E_k = -2\cos k$. The dotted line represents the Fermi energy determined by background particle fillings. There are three kinds of particles in our model, namely, the impurity particle (blue) and spin-↑ and spin-↓ particles (red). We consider the interaction between spin-↑ and spin-↓ particles, denoted U_{ff}, and the interaction between impurity and spin-↑ component, denoted U_{bf}.

where $\sigma = \uparrow, \downarrow$ denotes different spin species and $\hat{n}_{\mathbf{i}\sigma}$ is the density operator on the $\mathbf{i}$th lattice site. The operators $b^{\dagger}_{\mathbf{i}}$ and $b_{\mathbf{i}}$ represent the degrees of freedom of the impurity, which satisfy $\sum_{\mathbf{i}} b^{\dagger}_{\mathbf{i}} b_{\mathbf{i}} = 1$. This Hamiltonian contains two nearest-neighbor hopping parameters, t_{f} and t_{b}, and two on-site interactions, U_{ff} and U_{bf}. The chemical potential μ_{σ} is introduced to control the particle filling of background fermions, and we consider a spin-balanced case with $\mu_{\uparrow} = \mu_{\downarrow} = \mu$ and $N_{\uparrow} = N_{\downarrow} = N$. Both interacting parameters are negative ($U_{\mathrm{ff}}, U_{\mathrm{bf}} < 0$), corresponding to attractive interactions. We define the filling factor $\rho \equiv N/V$, with $V = L^D$ being the total number of sites (with half filling corresponding to $\rho = 1/2$). For all calculations below we use t_{f} and lattice constant a as the energy and length units, respectively, and fix $t_{\mathrm{b}} = t_{\mathrm{f}} = 1$.

First, we use the relations $c_{\mathbf{k}\sigma} = \frac{1}{\sqrt{V}} \sum_{\mathbf{i}} e^{-i\mathbf{k}\cdot\mathbf{i}} c_{\mathbf{i}\sigma}$ and $c^{\dagger}_{\mathbf{k}\sigma} = \frac{1}{\sqrt{V}} \sum_{\mathbf{i}} e^{i\mathbf{k}\cdot\mathbf{i}} c^{\dagger}_{\mathbf{i}\sigma}$ to rewrite the fermionic part of the Hamiltonian as

$$\begin{aligned}\hat{H} =& \sum_{\mathbf{k}\sigma} [\varepsilon_f(\mathbf{k}) - \mu_{\sigma}] c^{\dagger}_{\mathbf{k}\sigma} c_{\mathbf{k}\sigma} - t_b \sum_{\langle \mathbf{ij}\rangle} b^{\dagger}_{\mathbf{i}} b_{\mathbf{j}} \\ &+ \frac{U_{\mathrm{ff}}}{V} \sum_{\mathbf{k},\mathbf{k}',\mathbf{q}} c^{\dagger}_{\mathbf{k}\uparrow} c^{\dagger}_{\mathbf{q}-\mathbf{k}\downarrow} c_{\mathbf{q}-\mathbf{k}'\downarrow} c_{\mathbf{k}'\uparrow} \\ &+ \frac{U_{\mathrm{bf}}}{V} \sum_{\mathbf{i},\mathbf{k},\mathbf{k}'} e^{-i(\mathbf{k}-\mathbf{k}')\mathbf{i}} c^{\dagger}_{\mathbf{k}\uparrow} c_{\mathbf{k}'\uparrow} b^{\dagger}_{\mathbf{i}} b_{\mathbf{i}}, \end{aligned} \tag{2}$$

where the kinetic-energy dispersion of fermions is $\varepsilon_f(\mathbf{k}) = -2t_{\mathrm{f}}\cos k$ and $\varepsilon_f(\mathbf{k}) = -2t_{\mathrm{f}}(\cos k_x + \cos k_y)$ for 1D and 2D lattices, respectively.

We apply the Lee-Low-Pines (LLP) transformation to separate the degrees of freedom of the impurity and background. This unitary transformation is defined as $U_{\mathrm{LLP}} = e^{-i\hat{\mathbf{Q}}\hat{\mathbf{X}}}$, where $\hat{\mathbf{Q}} = \sum_{\mathbf{k}\sigma} \mathbf{k} c^{\dagger}_{\mathbf{k}\sigma} c_{\mathbf{k}\sigma}$ and $\hat{\mathbf{X}} = \sum_{\mathbf{i}} \mathbf{i} b^{\dagger}_{\mathbf{i}} b_{\mathbf{i}}$ are the total momentum operator of the background and the coordinate operator of the impurity, respectively. The operators transform as

$$\begin{aligned} U^{\dagger}_{\mathrm{LLP}} c_{\mathbf{k}\sigma} U_{\mathrm{LLP}} &= e^{-i\mathbf{k}\hat{\mathbf{X}}} c_{\mathbf{k}\sigma}, \\ U^{\dagger}_{\mathrm{LLP}} b_{\mathbf{i}} U_{\mathrm{LLP}} &= e^{-i\hat{\mathbf{Q}}\mathbf{i}} b_{\mathbf{i}}. \end{aligned} \tag{3}$$

Thus, the Hamiltonian after LLP transformation $\hat{H}_{\rm LLP} = U_{\rm LLP}^{\dagger}\hat{H}U_{\rm LLP}$ becomes

$$\begin{aligned}\hat{H}_{\rm LLP} =& \sum_{\mathbf{k},\sigma}(\varepsilon_f(\mathbf{k}) - \mu_\sigma)c_{\mathbf{k}\sigma}^{\dagger}c_{\mathbf{k}\sigma} \\ &- \sum_{\mathbf{k}} b_{\mathbf{k}}^{\dagger}b_{\mathbf{k}}\left[t_b\sum_{\boldsymbol{\delta}} e^{i(\mathbf{Q}-\mathbf{k})\cdot\boldsymbol{\delta}}\right] \\ &+ \frac{U_{\rm ff}}{V}\sum_{\mathbf{k},\mathbf{k}',\mathbf{q}} c_{\mathbf{k}\uparrow}^{\dagger}c_{\mathbf{q}-\mathbf{k}\downarrow}^{\dagger}c_{\mathbf{q}-\mathbf{k}'\downarrow}c_{\mathbf{k}'\uparrow} \\ &+ \sum_{\mathbf{k}} b_{\mathbf{k}}^{\dagger}b_{\mathbf{k}}\left(\frac{U_{\rm bf}}{V}\sum_{\mathbf{k}',\mathbf{k}''} c_{\mathbf{k}'\uparrow}^{\dagger}c_{\mathbf{k}''\uparrow}\right). \end{aligned} \tag{4}$$

Here, $\boldsymbol{\delta} = \pm 1$ for 1D and $\boldsymbol{\delta} \in \{(\pm 1, 0), (0, \pm 1)\}$ for 2D lattices are the unit lattice vectors, respectively, and we use the Fourier transformation of impurity operators $b_{\mathbf{k}} = \frac{1}{\sqrt{V}}\sum_{\mathbf{i}} e^{-i\mathbf{k}\cdot\mathbf{i}}b_{\mathbf{i}}$ and $b_{\mathbf{k}}^{\dagger} = \frac{1}{\sqrt{V}}\sum_{\mathbf{i}} e^{i\mathbf{k}\cdot\mathbf{i}}b_{\mathbf{i}}^{\dagger}$. One can easily prove that the momenta of the background and impurity transform as $U_{\rm LLP}^{\dagger}\hat{\mathbf{Q}}U_{\rm LLP} = \hat{\mathbf{Q}}$ and $U_{\rm LLP}^{\dagger}(\sum_{\mathbf{k}}\mathbf{k}b_{\mathbf{k}}^{\dagger}b_{\mathbf{k}})U_{\rm LLP} = \sum_{\mathbf{k}}\mathbf{k}b_{\mathbf{k}}^{\dagger}b_{\mathbf{k}} - \hat{\mathbf{Q}}$, respectively. Thus, the conserved total momentum of the original mode is transformed to that of the impurity,

$$U_{\rm LLP}^{\dagger}\left(\sum_{\mathbf{k}}\mathbf{k}b_{\mathbf{k}}^{\dagger}b_{\mathbf{k}} + \hat{\mathbf{Q}}\right)U_{\rm LLP} = \sum_{\mathbf{k}}\mathbf{k}b_{\mathbf{k}}^{\dagger}b_{\mathbf{k}}. \tag{5}$$

Thus, for a given total momentum $\mathbf{K}$, the ground state of $\hat{H}_{\rm LLP}$ can be written in the form of a direct product of the impurity part and the background part as $b_{\mathbf{K}}^{\dagger}|0\rangle \otimes |\Psi_{\mathbf{K}}\rangle$. With the number constraint $\sum_{\mathbf{k}} b_{\mathbf{k}}^{\dagger}b_{\mathbf{k}} = 1$, we obtain the Hamiltonian of background fermions with a fixed total momentum $\mathbf{K}$,

$$\begin{aligned}\hat{H}_{\mathbf{K}} =& \sum_{\mathbf{k},\sigma}[\varepsilon_f(\mathbf{k}) - \mu_\sigma]c_{\mathbf{k}\sigma}^{\dagger}c_{\mathbf{k}\sigma} - t_b\sum_{\boldsymbol{\delta}} e^{i(\mathbf{Q}-\mathbf{K})\cdot\boldsymbol{\delta}} \\ &+ \frac{U_{\rm ff}}{V}\sum_{\mathbf{k},\mathbf{k}',\mathbf{q}} c_{\mathbf{k}\uparrow}^{\dagger}c_{\mathbf{q}-\mathbf{k}\downarrow}^{\dagger}c_{\mathbf{q}-\mathbf{k}'\downarrow}c_{\mathbf{k}'\uparrow} + \frac{U_{\rm bf}}{V}\sum_{\mathbf{k},\mathbf{k}'} c_{\mathbf{k}\uparrow}^{\dagger}c_{\mathbf{k}'\uparrow}. \end{aligned} \tag{6}$$

We denote the ground state of $\hat{H}_{\mathbf{K}}$ as $|\Psi_{\mathbf{K}}\rangle$, and the ground state of the original Hamiltonian (2) can be expressed as $|\Psi\rangle = U_{\rm LLP}(b_{\mathbf{K}}^{\dagger}|0\rangle \otimes |\Psi_{\mathbf{K}}\rangle)$. Note that after the LLP transformation, the impurity and background are separated, and the polaron problem is mapped exactly to finding the ground state of a two-component Fermi gas with an impurity-modified interaction. In general, the modified interaction is long range and acquires a complex form.

To solve for $|\Psi_{\mathbf{K}}\rangle$, next, we use a fermionic Gaussian state as a trial wave function, which has the form

$$|\Psi_{\rm GS}\rangle = \hat{U}_{\rm GS}|0\rangle, \tag{7}$$

where $\hat{U}_{\rm GS} = e^{i\frac{1}{4}\hat{\mathbf{A}}^T\boldsymbol{\xi}\hat{\mathbf{A}}}$ is an Gaussian unitary operator. The operator vector $\hat{\mathbf{A}} = (a_{1,\mathbf{k}_1}^{\uparrow}, \ldots, a_{1,\mathbf{k}_V}^{\uparrow}, a_{1,\mathbf{k}_1}^{\downarrow}, \ldots, a_{1,\mathbf{k}_V}^{\downarrow}, a_{2,\mathbf{k}_1}^{\uparrow}, \ldots, a_{2,\mathbf{k}_V}^{\uparrow}, a_{2,\mathbf{k}_1}^{\downarrow}, \ldots, a_{2,\mathbf{k}_V}^{\downarrow})^T$ is defined via the Majorana operators $a_{1,\mathbf{k}_j}^{\sigma} = c_{\mathbf{k}_j,\sigma}^{\dagger} + c_{\mathbf{k}_j,\sigma}$ and $a_{2,\mathbf{k}_j}^{\sigma} = i(c_{\mathbf{k}_j,\sigma}^{\dagger} - c_{\mathbf{k}_j,\sigma})$, which satisfy the anticommutation relation $\{a_{\alpha,\mathbf{k}}^{\sigma}, a_{\beta,\mathbf{k}'}^{\sigma'}\} = 2\delta_{\alpha\beta}\delta_{\mathbf{k},\mathbf{k}'}\delta_{\sigma\sigma'}$. The variational parameter $\boldsymbol{\xi}$ is an antisymmetric Hermitian matrix. To eliminate the gauge degree of freedom, we can relate $\boldsymbol{\xi}$ to a covariant matrix $\boldsymbol{\gamma}$ via $\boldsymbol{\gamma} = \mathbf{P}\boldsymbol{\Omega}\mathbf{P}^T$, where the covariant matrix is defined as [33]

$$\gamma_{i,j} = \frac{i}{2}\langle\Psi_{\rm GS}\,|[\hat{A}_i, \hat{A}_j]|\Psi_{\rm GS}\rangle, \tag{8}$$

with $\hat{A}_i$ being the ith element of $\hat{\mathbf{A}}$, $\mathbf{P} = e^{i\boldsymbol{\xi}}$, and the symplectic matrix $\boldsymbol{\Omega}$ being

$$\boldsymbol{\Omega} = \begin{pmatrix} \mathbf{0} & -\mathbf{1}_{2V} \\ \mathbf{1}_{2V} & \mathbf{0} \end{pmatrix}. \tag{9}$$

Next, we calculate the variational parameters of the Gaussian state. For a given initial state $|\Psi(0)\rangle$, we can determine the ground state of a Hamiltonian $\hat{H}$ via the imaginary-time evolution

$$|\Psi(\tau)\rangle = \frac{e^{-\hat{H}\tau}|\Psi(0)\rangle}{\sqrt{\langle\Psi(0)|e^{-2\hat{H}\tau}|\Psi(0)\rangle}} \tag{10}$$

in the asymptotic limit $\tau \to \infty$, as long as $|\Psi(0)\rangle$ has a nonzero overlap with the ground state. Such an evolution can be described by a differential equation,

$$d_\tau|\Psi(\tau)\rangle = -(\hat{H} - \langle\hat{H}\rangle)|\Psi(\tau)\rangle, \tag{11}$$

with $\langle\hat{H}\rangle = \langle\Psi(\tau)|\hat{H}|\Psi(\tau)\rangle$. The imaginary-time evolution equation for the Gaussian state (7) can be written as

$$d_\tau|\Psi_{\rm GS}\rangle = -\hat{\mathcal{P}}(\hat{H} - E)|\Psi_{\rm GS}\rangle, \tag{12}$$

where $E = \langle\Psi_{\rm GS}|\hat{H}|\Psi_{\rm GS}\rangle$ is the variational energy and $\hat{\mathcal{P}}$ is the projection operator onto the subspace spanned by tangent vectors of the variational manifold. The left-hand side of Eq. (12) gives

$$d_\tau|\Psi_{\rm GS}\rangle = \hat{U}_{\rm GS}\hat{U}_L|0\rangle, \tag{13}$$

where the operator $\hat{U}_L$ is given by

$$\hat{U}_L = \frac{1}{4}{:}\hat{\mathbf{A}}^T\mathbf{P}^T(\partial_\tau\mathbf{P})\hat{\mathbf{A}}{:} + \frac{i}{4}\mathrm{Tr}[\mathbf{P}^T(\partial_\tau\mathbf{P})\boldsymbol{\gamma}] \tag{14}$$

and $:\cdot:$ represents normal ordering with respect to the vacuum state. The right-hand side of Eq. (12) further reads

$$-(\hat{H} - \langle\hat{H}\rangle)|\Psi_{\rm GS}\rangle = -\hat{U}_{\rm GS}\hat{U}_R|0\rangle, \tag{15}$$

where $\hat{U}_R = (i/4){:}\hat{\mathbf{A}}^T\mathbf{P}^T\mathbf{h}\mathbf{P}\hat{\mathbf{A}}{:} + \delta\hat{H}$. Here, $\delta\hat{H}$ denotes the higher-order terms of $c_{\mathbf{k}\sigma}$ which are orthogonal to the tangential space and about to be projected out by the $\hat{\mathcal{P}}$ operator in Eq. (12), and

$$\mathbf{h} = 4\frac{\delta E}{\delta\boldsymbol{\gamma}}, \tag{16}$$

is the functional derivative of the variational energy. Comparing Eqs. (13) and (15), we can finally obtain the imaginary-time equation of motion for the covariance matrix as [33,52]

$$\partial_\tau\boldsymbol{\gamma} = -\mathbf{h} - \boldsymbol{\gamma}\mathbf{h}\boldsymbol{\gamma}. \tag{17}$$

We can determine the covariance matrix of the final state according to Eq. (17). First, we need to calculate the functional derivative $\mathbf{h}$ defined in Eq. (16). To accomplish that, we

rewrite the Hamiltonian (6) with Majorana operators as

$$\begin{aligned} H_{\mathbf{K}} = & \frac{1}{4}\sum_{\mathbf{k}\sigma}[\varepsilon_f(\mathbf{k})-\mu_\sigma]\big(2+ia^\sigma_{1,\mathbf{k}}a^\sigma_{2,\mathbf{k}}-ia^\sigma_{2,\mathbf{k}}a^\sigma_{1,\mathbf{k}}\big)-t_b\sum_\delta e^{i(\mathbf{Q}-\mathbf{K})\delta} \\ & + \frac{U_{\mathrm{bf}}}{4V}\sum_{\mathbf{k},\mathbf{k}'}(a^\uparrow_{1,\mathbf{k}}a^\uparrow_{1,\mathbf{k}'}+a^\uparrow_{2,\mathbf{k}}a^\uparrow_{2,\mathbf{k}'}+ia^\uparrow_{1,\mathbf{k}}a^\uparrow_{2,\mathbf{k}'}-ia^\uparrow_{2,\mathbf{k}}a^\uparrow_{1,\mathbf{k}'}) \\ & + \frac{U_{\mathrm{ff}}}{16V}\sum_{\mathbf{k},\mathbf{k}',\mathbf{q}}(a^\uparrow_{1\mathbf{k}}-ia^\uparrow_{2\mathbf{k}})(a^\downarrow_{1\mathbf{q}-\mathbf{k}}-ia^\downarrow_{2\mathbf{q}-\mathbf{k}})(a^\downarrow_{1\mathbf{q}-\mathbf{k}'}+ia^\downarrow_{2\mathbf{q}-\mathbf{k}'})(a^\uparrow_{1\mathbf{k}'}+ia^\uparrow_{2\mathbf{k}'}). \end{aligned} \tag{18}$$

Then using the formula of expectation under the fermionic Gaussian state

$$i^p\langle a_{j_1}\cdots a_{j_{2p}}\rangle_{\mathrm{GS}} = \mathrm{Pf}\big([\boldsymbol{\gamma}]_{j_1\cdots j_{2p}}\big), \tag{19}$$

where $1\leqslant j_1<\cdots<j_{2p}\leqslant 4V$ and $\mathrm{Pf}([\boldsymbol{\gamma}]_{j_1\cdots j_{2p}})$ denotes the Pfaffian of the antisymmetric matrix $[\boldsymbol{\gamma}]_{j_1\cdots j_{2p}}$ with rows and columns $j_1,\ldots,j_{2p}$ of $\boldsymbol{\gamma}$, we can calculate the variational energy $E=\langle\Psi_{\mathrm{GS}}|\hat{H}_{\mathbf{K}}|\Psi_{\mathrm{GS}}\rangle$ and the functional derivative of the variational energy $\mathbf{h}=4\delta E/\delta\boldsymbol{\gamma}$. More details of the derivation are summarized in Appendixes A and B.

By evolving Eq. (17) until a convergence of variational energy E is reached, we get the covariant matrix $\boldsymbol{\gamma}$ of the ground state. With that we can compute various physical observables, such as the total particle number

$$\begin{aligned} N_{\mathrm{total}} &= \sum_\sigma N_\sigma = -\sum_\sigma \frac{\partial E}{\partial\mu_\sigma} \\ &= V-\frac{1}{4}\sum_{i,j}\Omega_{i,j}\gamma_{i,j}, \end{aligned} \tag{20}$$

where $\Omega_{i,j}$ is the element of the symplectic matrix defined in Eq. (9). We can also calculate the double occupancy of the background component, defined as

$$d=\frac{1}{V}\sum_{\mathbf{i}}\langle c^\dagger_{\mathbf{i}\uparrow}c^\dagger_{\mathbf{i}\downarrow}c_{\mathbf{i}\downarrow}c_{\mathbf{i}\uparrow}\rangle, \tag{21}$$

which describes the short-range pairing correlations of the ground state and can be measured via *in situ* imaging [51] and time-of-flight techniques [53,54]. We need to substitute the operators in Eq. (21) by Majorana operators and combine them with Eq. (19) to obtain the numerical result of d using the covariant matrix. A detailed calculation is given in Appendix C.

III. GROUND-STATE ENERGY AND DOUBLE OCCUPANCY

Since the background of the two-component Fermi gas undergoes a BCS-BEC crossover, it is natural to assume a BCS wave function for the variational initial state, which has a Gaussian form and comprises the pairing effect based on the BCS theory of superconductivity. The standard form of this state is [55]

$$\big|\Psi^{(\bar{N})}_{\mathrm{Gauss}}\big\rangle=\prod_k(u_k+v_ka^\dagger_ka^\dagger_{-k})|0\rangle, \tag{22}$$

where $k\equiv(\mathbf{k},\uparrow)$ and $-k\equiv(-\mathbf{k},\downarrow)$ are defined to simplify notation and $\bar{N}=\sum_k\langle a^\dagger_ka_k\rangle=2\sum_k|v_k|^2$ stands for the number of pairs. The parameters u_k and v_k are random numbers satisfying $|u_k|^2+|v_k|^2=1$. The advantage of using the BCS wave function as a variational state is that it naturally fixes the particle number of two background components to be the same. We can also use a random Gaussian form as the initial state and impose the number constraint during imaginary-time evolution. For all parameters discussed below, the same final state is obtained, but with a much longer time to reach convergence.

First, we apply the non-Gaussian method to study the extremely dilute limit of 1D and 2D square lattices with the periodic boundary condition, where only two fermions are present in the background. This can be done by changing the chemical potentials, such that the particle numbers of background fermions are tuned to $N_\uparrow=N_\downarrow=1$ after convergence. In this limit, the polaron problem reduces to a three-particle model with one particle (spin $\uparrow$) interacting with the other two noninteracting particles (impurity and spin $\downarrow$), and the ground state can easily be solved by other analytic or numerical methods to benchmark the non-Gaussian algorithm. In particular, if we turn off either of the interactions, the system further reduces to a two-body problem with an add-on free atom. The ground state can be solved analytically, leading to the equation

$$-\frac{V}{U}=\sum_{\mathbf{k}}\frac{1}{2\varepsilon'_{\mathbf{k}}+E_b}. \tag{23}$$

Here, the energy dispersion is shifted to $\varepsilon'_{\mathbf{k}}=2D-2\cos\mathbf{k}$. The binding energy E_b is defined as the absolute value of the two-body ground-state energy. In Figs. 2(a) and 2(b), we show the two-body binding energy E_b obtained from Eq. (23) as solid black lines in one and two dimensions, respectively, along with the corresponding numerical results obtained using the non-Gaussian variational method. In these plots, red crosses and blue circles represent the cases with $U_{\mathrm{ff}}=U, U_{\mathrm{bf}}=0$ and $U_{\mathrm{bf}}=U, U_{\mathrm{ff}}=0$, respectively. The system size is taken as $L=60$ for 1D lattices and $L=10$ for 2D lattices. We find that the numerical results agree well with the analytical ones for both cases, especially in the strongly interacting limit.

For a genuine three-body system with $U_{\mathrm{bf}}\neq 0$ and $U_{\mathrm{ff}}\neq 0$ in 1D lattices, we can use the density-matrix renormalization-group algorithm based on matrix product states (MPSs) to determine the ground-state energy, with system size $L=60$ and a maximum bond dimension up to $M=1600$. In Fig. 2(c) we show the ground-state energy obtained via the

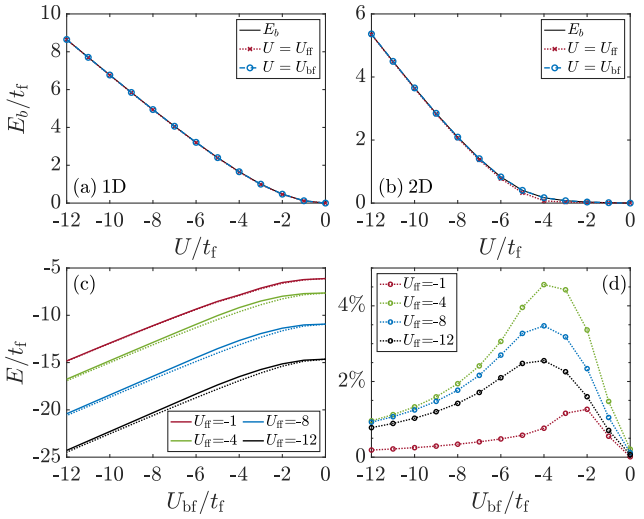

FIG. 2. Two-body binding energy for (a) a 1D chain with size $L = 60$ and (b) a 2D square lattice with $L = 10$. Exact solutions for both cases are obtained by solving Eq. (23) numerically in the thermodynamic limit. Here, we turn on only one interaction and fix the other one to be zero. The markers here represent $U = U_{ff}$ (red crosses) and $U = U_{bf}$ (blue circles). (c) The three-body ground-state energy versus U_{bf}, with different U_{ff}: -1 (red), -4 (green), -8 (blue), and -12 (black). The dotted lines are corresponding ground-state energies obtained using the MPS method. (d) The systematic errors for the three-body energy, defined as $|E_{MPS} - E|/|E_{MPS}|$.

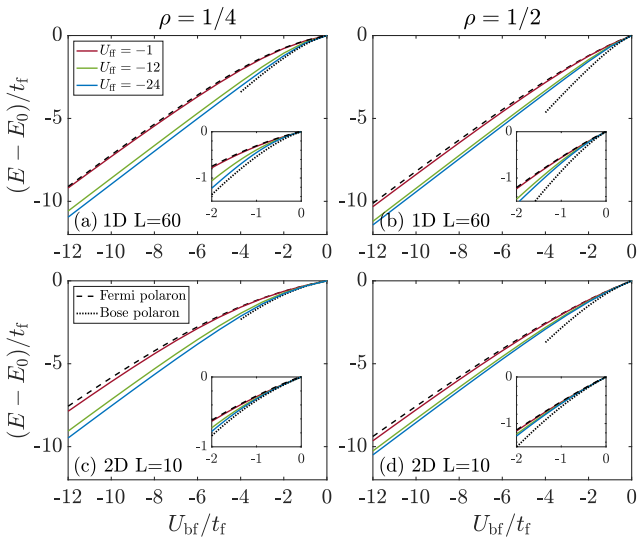

FIG. 3. The polaron energy [shifted by $E_0 = E(U_{bf} = 0)$] for 1D and 2D systems, with particle fillings $\rho = 1/4$ and $\rho = 1/2$. The system size is $L = 60$ for the 1D case and $L = 10$ for the 2D case. The black dashed and dotted lines represent the Fermi-polaron and Bose-polaron energies obtained using the Chevy-like ansatz, respectively. The behavior within the weak-U_{bf} limit is closely shown in the insets. With increasing background interaction $U_{ff} = -1, -12, -24$, we observe the polaron energy of our model go through a smooth crossover between two limits for both 1D and 2D systems.

non-Gaussian variational approach (solid lines) and the MPS method (dotted lines). The background interaction is fixed as $U_{ff} = -1$ (red), -4 (green), -8 (blue), and -12 (black). We find that the discrepancy between the two methods is very small in both the weak- and strong-interaction limits and reaches the maximum around $U_{bf} \approx -4$. This conclusion can be seen more clearly in Fig. 2(d), where the relative error $|E_{MPS} - E|/E_{MPS}$ is displayed. We see that the error reaches the highest value of $\sim$4.5% for $U_{ff} \sim -4$ and $U_{bf} \sim -4$, where the system is undergoing the crossover regime, with the interaction energy of the system being qualitatively comparable to the kinetic energy characterized by the bandwidth. These results indicate the validity of the non-Gaussian variational method.

We now investigate the polaron problem with different fillings ρ of the Fermi background. For definiteness, we consider the cases with $\rho = N/V = 1/4$ and $1/2$ as representative examples. In the BCS limit of $U_{ff} \to 0$, the system reduces to a single-component Fermi-polaron problem, where the impurity interacts only with spin-$\uparrow$ atoms, and the spin-$\downarrow$ component supplies only an energy shift for the total ground-state energy. With increasing background interaction U_{ff}, spin-$\uparrow$ and spin-$\downarrow$ particles start to form tightly bound pairs. In the BEC limit with $|U_{ff}| \gg (|U_{bf}|, t_f)$, the presence of an impurity will not break the background pairs; it will interact with the pair as a whole to form a Bose polaron.

In Fig. 3 we plot the variational ground-state energy varying with $U_{bf} \in [-12, 0]$, with different background interactions, $U_{ff} = -1$ (red), -12 (green), and -24 (blue). For small U_{ff}, the ground-state energy obtained with the non-Gaussian method is compared with that of a Fermi polaron with $m_{imp}/m_{bath} = 1$ (black dashed lines), which is obtained by using a Chevy-like ansatz of one particle-hole fluctuations and zero center-of-mass momentum [35],

$$|\Psi\rangle = \psi_0 b_{\mathbf{0}}^\dagger |N\rangle_\uparrow + \sum_{\mathbf{k},\mathbf{q}} \psi_{\mathbf{kq}} b_{\mathbf{q}-\mathbf{k}}^\dagger c_{\mathbf{k}\uparrow}^\dagger c_{\mathbf{q}\uparrow} |N\rangle_\uparrow. \tag{24}$$

Here, $b_{\mathbf{k}}$ and $c_{\mathbf{k}\uparrow}$ are the field operators for the impurity and background fermions, respectively. The summation over $\mathbf{k}$ ($\mathbf{q}$) is restricted above (below) the Fermi surface. As shown in all panels of Fig. 3, the non-Gaussian results approach the Fermi-polaron limit from below with decreasing U_{ff} for all lattice configurations and filling factors.

With increasing background attraction U_{ff}, the polaron energy is overall reduced as one would naturally anticipated. However, the reduction is nonuniform, with a large difference between $U_{ff} = -1$ and -12 but a small change from $U_{ff} = -12$ to -24. A rather unexpected observation is that even for the case of strongest Hubbard attraction ($U_{ff} = -24$) considered, the energy lies well above the limit of the Bose polaron (black dotted lines) except for a very small impurity-background interaction. Here, the Bose-polaron energy is calculated for an impurity coupling to a noninteracting Bose gas of molecules with hopping parameter t_m and interaction U_{bm} via a Chevy-like ansatz with first-order fluctuations [37],

$$|\Psi\rangle = \left(\psi_0 b_{\mathbf{0}}^\dagger + \sum_{\mathbf{k}} \psi_{\mathbf{k}} b_{-\mathbf{k}}^\dagger \beta_{\mathbf{k}}^\dagger\right)|\mathrm{BEC}\rangle. \tag{25}$$

Here, $\beta_{\mathbf{k}}^\dagger$ creates a Bogoliubov mode with momentum $\mathbf{k}$, and $|\mathrm{BEC}\rangle$ represents the ground state of the BEC with zero center of momentum, which satisfies $\beta_{\mathbf{k}}|\mathrm{BEC}\rangle = 0$. If we consider

a very small on-site molecule-molecule repulsion $U_{\rm m}$, the energy equation obtained from this trial wave function is [37]

$$\frac{E}{N}=\left\{\frac{V}{U_{\rm bm}}-\sum_{\mathbf{k}}\frac{u_{\mathbf{k}}^2}{E-\varepsilon_{\rm b}(-\mathbf{k})-E_{\rm m}(\mathbf{k})}\right\}^{-1}, \tag{26}$$

with $u_{\mathbf{k}}^2=[(\varepsilon_m(\mathbf{k})^2+\rho U_{\rm m})/E_{\rm m}(\mathbf{k})+1]/2$ and excitation spectrum $E_{\rm m}(\mathbf{k})=\sqrt{\varepsilon_m(\mathbf{k})^2+2\varepsilon_m(\mathbf{k})\rho U_{\rm m}}$. The energy dispersions for the impurity and molecule are $\varepsilon_b(\mathbf{k})=2D-2t_b\cos(\mathbf{k})$ and $\varepsilon_m(\mathbf{k})=2D-2t_m\cos(\mathbf{k})$, respectively.

In Fig. 3, we show the Bose-polaron energy shifted by the zero-point value in the noninteracting limit with $t_m=1/2$, which corresponds to a background of molecules with two times the mass of the impurity, i.e., $m_{\rm imp}/m_{\rm bath}=1/2$, and interaction $U_{\rm bm}=U_{\rm bf}$. This result indicates that the Bose-polaron limit can be reached only for sufficiently weak impurity-background interaction, even when the attraction of background fermions is strong enough to reach the BEC limit of the BCS-BEC crossover. This observation can be understood by noticing that the impurity-background interaction is, in fact, a many-body effect, in which all spin-↑ fermions take parts. Thus, a small $U_{\rm bf}$ can also cause significant change to the ground state after we count the contributions from all fermions. Indeed, if we increase the number of fermions from $\rho=1/4$ to $1/2$, the difference between the variational results and the Bose-polaron limit is notably enlarged with the same values of $U_{\rm ff}$ and $U_{\rm bf}$. Notice that in all panels in Fig. 3, the interaction between bosonic molecules is assumed to be zero, $U_{\rm m}=0$. This simplification can be justified by a recent work [56] that found that there is no distinguishable difference between polaron energies obtained with interacting and noninteracting backgrounds in the weak impurity-background interaction limit. Further, the variational energy of the Bose polaron given by the Chevy-like ansatz is proved to be in good agreement with the outcome of quantum Monte Carlo [57] in a 2D continuum within the weak impurity-background coupling regime.

Finally, we calculate the double occupancy d of background fermions by changing the interactions $U_{\rm ff}$ and $U_{\rm bf}$ using the method described in detail in Appendix C. The results in Fig. 4 show little difference for different choices of impurity-background interaction $U_{\rm bf}$ or from those of a simple attractive Hubbard model [58] with no presence of impurity. This suggests that the background wave function is essentially not perturbed by the impurity. While the double occupancy has been successfully used to characterize the BCS-BEC crossover of the background [58], it cannot work as a good measure for the Fermi-Bose-polaron crossover. We show momentum distributions for both the 1D and 2D cases in Fig. 5, which suggest that the background undergoes a BCS-BEC crossover with increasing $U_{\rm ff}$. The impurity background interaction is fixed at $U_{\rm bf}=-12$; these results suggest that an impurity would cause a discernible difference between $n_\uparrow$ and $n_\downarrow$ for $U_{\rm bf}\ll U_{\rm ff}$, whereas $n_\downarrow$ is always near the Hubbard model results. The inset in Fig. 5(b) is a 1D example for the Bose-polaron limit $U_{\rm bf}=-1$, $U_{\rm ff}=-24$, where the impurity has no major effect on the background momentum distributions. Although we have successfully determined the background wave function, the measurement of the Fermi-Bose-polaron crossover needs to be achieved by calculating the impurity momentum distribution or impurity-background correlation, which remains difficult for all types of approaches.

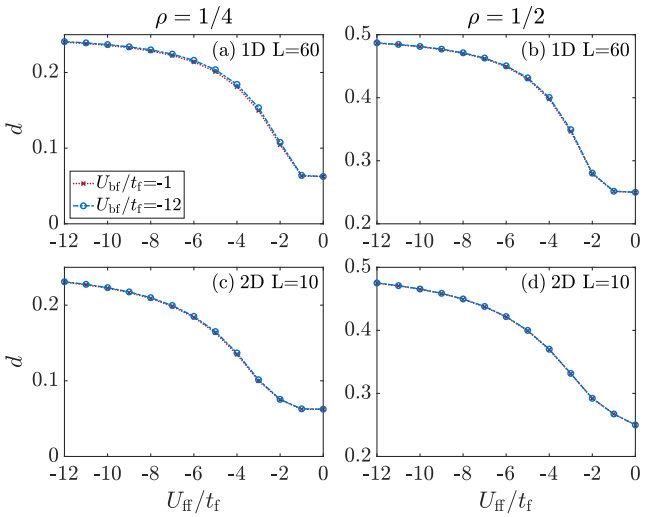

FIG. 4. Double occupancy d for one- and two-dimensional square lattices with different particle fillings $\rho=1/4$ and $\rho=1/2$, and impurity-background interactions, $U_{\rm bf}=-1$ (red crosses) and -12 (blue circles), varying with background interaction $U_{\rm ff}$.

IV. CONCLUSION

In summary, we presented a non-Gaussian variational calculation for the ground-state properties of a polaron problem with an interacting background in one- and two-dimensional

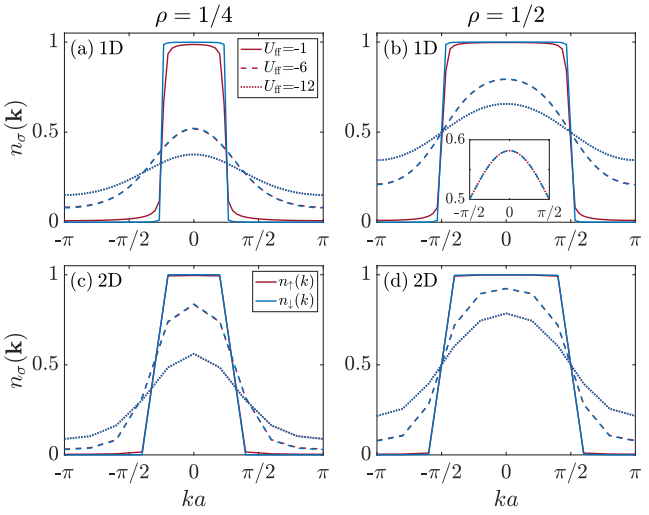

FIG. 5. Momentum distribution $n_\sigma(\mathbf{k})$ for one- and two-dimensional square lattices with different particle fillings: $\rho=1/4$ and $\rho=1/2$. The 1D and 2D results are plotted along $k=k_x$ and $k=k_x=k_y$. We choose three different background interactions, $U_{\rm ff}=-1,-6,-12$, represented by solid, dashed, and dotted lines, respectively, while the impurity-background interaction is fixed as $U_{\rm bf}=-12$. The inset of (b) shows the 1D momentum distribution for the Bose-polaron limit $U_{\rm bf}=-1$, $U_{\rm ff}=-24$.

square lattices. We obtained the ground-state covariant matrix via imaginary-time evolution and then computed the total energy, background double occupancy, and momentum distribution of this system. The energy results showed that with increasing background interaction strength, the system undergoes a smooth crossover from a Fermi-polaron to Bose-polaron system. From the double occupancy and momentum distribution we found that the existence of an impurity will not significantly affect the background pairs. We can easily expand our system to a mass- or spin-imbalanced case by adjusting the hopping parameter or chemical potential in the original Hamiltonian, which can be used to investigate impurity physics on lattice systems of interest in quantum simulations [59,60]. Moreover, the computations do not depend on the dimensionality or form of the lattice and can be directly applied to various types of lattice configurations in different dimensions. The non-Gaussian variational method can be further used to study the real-time evolution to describe out-of-equilibrium dynamics.

ACKNOWLEDGMENTS

We thank Tao Shi for helpful discussions. This work is supported by the National Key R&D Program of China (Grant No. 2022YFA1405301) and the National Natural Science Foundation of China (Grants No. 12074428 and No. 92265208). Y.-R.S. acknowledges the Postdoctoral Fellowship Program of China Postdoctoral Science Foundation (Grant No. GZC20232775).

APPENDIX A: VARIATIONAL ENERGY

We use the expression given in Eq. (18) to determine the variational energy $E = \langle \Psi_{\mathrm{GS}}|H|\Psi_{\mathrm{GS}}\rangle$, leading to

$$
\begin{aligned}
E = &\left\langle \frac{1}{4}\sum_{\mathbf{k}\sigma}[\varepsilon_f(\mathbf{k})-\mu_\sigma]\big(2+ia^\sigma_{1,\mathbf{k}}a^\sigma_{2,\mathbf{k}}-ia^\sigma_{2,\mathbf{k}}a^\sigma_{1,\mathbf{k}}\big)-t_b\sum_\delta e^{i(\mathbf{Q}-\mathbf{K})\delta}\right.\\
&+\frac{U_{\mathrm{bf}}}{4V}\sum_{\mathbf{k},\mathbf{k}'}(a^\uparrow_{1,\mathbf{k}}a^\uparrow_{1,\mathbf{k}'}+a^\uparrow_{2,\mathbf{k}}a^\uparrow_{2,\mathbf{k}'}+ia^\uparrow_{1,\mathbf{k}}a^\uparrow_{2,\mathbf{k}'}-ia^\uparrow_{2,\mathbf{k}}a^\uparrow_{1,\mathbf{k}'})\\
&\left.+\frac{U_{\mathrm{ff}}}{16V}\sum_{\mathbf{k},\mathbf{k}',\mathbf{q}}(a^\uparrow_{1\mathbf{k}}-ia^\uparrow_{2\mathbf{k}})(a^\downarrow_{1\mathbf{q}-\mathbf{k}}-ia^\downarrow_{2\mathbf{q}-\mathbf{k}})(a^\downarrow_{1\mathbf{q}-\mathbf{k}'}+ia^\downarrow_{2\mathbf{q}-\mathbf{k}'})(a^\uparrow_{1\mathbf{k}'}+ia^\uparrow_{2\mathbf{k}'})\right\rangle_{\mathrm{GS}}\\
=&\frac{1}{2}\sum_{\mathbf{k}\sigma}[\varepsilon_f(\mathbf{k})-\mu_\sigma]+\frac{1}{4}\sum_{\mathbf{k}\sigma}[\varepsilon_f(\mathbf{k})-\mu_\sigma](\gamma_{1,\mathbf{k}\sigma;2,\mathbf{k}\sigma}-\gamma_{2,\mathbf{k}\sigma;1,\mathbf{k}\sigma})-t_b\sum_{\boldsymbol{\delta}}e^{-i\mathbf{K}\cdot\boldsymbol{\delta}}\left(-\frac{1}{2}\right)^{2N_s}s_f\mathrm{Pf}(\gamma_F)\\
&+\frac{U_{\mathrm{bf}}}{2}+\frac{U_{\mathrm{bf}}}{4V}\sum_{\mathbf{k},\mathbf{k}'}(\gamma_{1,\mathbf{k}\uparrow;2,\mathbf{k}'\uparrow}-\gamma_{2,\mathbf{k}\uparrow;1,\mathbf{k}'\uparrow})+\frac{VU_{\mathrm{ff}}}{4}+\frac{U_{\mathrm{ff}}}{8}\sum_{\mathbf{k}}(\gamma_{1,\mathbf{k},\uparrow;2,\mathbf{k},\uparrow}+\gamma_{1,\mathbf{k},\downarrow;2,\mathbf{k},\downarrow}-\gamma_{2,\mathbf{k},\downarrow;1,\mathbf{k},\downarrow}-\gamma_{2,\mathbf{k},\uparrow;1,\mathbf{k},\uparrow})\\
&+\frac{U_{\mathrm{ff}}}{16V}\sum_{\mathbf{k},\mathbf{k}',\mathbf{q}}[(\gamma_{1,\mathbf{k},\uparrow;1,\mathbf{q}-\mathbf{k},\downarrow}-\gamma_{2,\mathbf{k},\uparrow;2,\mathbf{q}-\mathbf{k},\downarrow})(\gamma_{2,\mathbf{q}-\mathbf{k}',\downarrow;2,\mathbf{k}',\uparrow}-\gamma_{1,\mathbf{q}-\mathbf{k}',\downarrow;1,\mathbf{k}',\uparrow})\\
&+(\gamma_{1,\mathbf{k},\uparrow;1,\mathbf{q}-\mathbf{k}',\downarrow}+\gamma_{2,\mathbf{k},\uparrow;2,\mathbf{q}-\mathbf{k}',\downarrow})(\gamma_{1,\mathbf{q}-\mathbf{k},\downarrow;1,\mathbf{k}',\uparrow}+\gamma_{2,\mathbf{q}-\mathbf{k},\downarrow;2,\mathbf{k}',\uparrow})\\
&-(\gamma_{1,\mathbf{k},\uparrow;1,\mathbf{k}',\uparrow}+\gamma_{2,\mathbf{k},\uparrow;2,\mathbf{k}',\uparrow})(\gamma_{1,\mathbf{q}-\mathbf{k},\downarrow;1,\mathbf{q}-\mathbf{k}',\downarrow}+\gamma_{2,\mathbf{q}-\mathbf{k},\downarrow;2,\mathbf{q}-\mathbf{k}',\downarrow})\\
&+(\gamma_{1,\mathbf{k},\uparrow;2,\mathbf{q}-\mathbf{k}',\downarrow}-\gamma_{2,\mathbf{k},\uparrow;1,\mathbf{q}-\mathbf{k}',\downarrow})(\gamma_{2,\mathbf{q}-\mathbf{k},\downarrow;1,\mathbf{k}',\uparrow}-\gamma_{1,\mathbf{q}-\mathbf{k},\downarrow;2,\mathbf{k}',\uparrow})\\
&-(\gamma_{1,\mathbf{k},\uparrow;2,\mathbf{q}-\mathbf{k},\downarrow}+\gamma_{2,\mathbf{k},\uparrow;1,\mathbf{q}-\mathbf{k},\downarrow})(\gamma_{1,\mathbf{q}-\mathbf{k}',\downarrow;2,\mathbf{k}',\uparrow}+\gamma_{2,\mathbf{q}-\mathbf{k}',\downarrow;1,\mathbf{k}',\uparrow})\\
&+(\gamma_{1,\mathbf{k},\uparrow;2,\mathbf{k}',\uparrow}-\gamma_{2,\mathbf{k},\uparrow;1,\mathbf{k}',\uparrow})(\gamma_{1,\mathbf{q}-\mathbf{k},\downarrow;2,\mathbf{q}-\mathbf{k}',\downarrow}-\gamma_{2,\mathbf{q}-\mathbf{k},\downarrow;1,\mathbf{q}-\mathbf{k}',\downarrow})],
\end{aligned}
\tag{A1}
$$

where $\gamma_F=\sqrt{1-e^{i\alpha}}\gamma\sqrt{1-e^{i\alpha}}-(1+e^{i\alpha})\Sigma$, $\alpha=\mathbb{1}_4\otimes\mathrm{diag}(\mathbf{k}\cdot\boldsymbol{\delta})$, $\mathrm{diag}(\mathbf{k}\cdot\boldsymbol{\delta})$ is a diagonal matrix with diagonal elements $\mathbf{k}_1\cdot\boldsymbol{\delta},\ldots,\mathbf{k}_{N_s}\cdot\boldsymbol{\delta}$, and $\mathrm{Pf}(\gamma_F)$ denotes the Pfaffian of γ_F. The energy we show in the main text is obtained via this expression.

APPENDIX B: DERIVATIVE OF THE VARIATIONAL ENERGY

After we get Eq. (A1), we can calculate the functional derivative $h=4\delta E/\delta\gamma$. The element of matrix h can be expressed as $h_{s_1,\mathbf{k_1},\sigma_1;s_2,\mathbf{k_2},\sigma_2}=4\delta E/\delta\gamma_{s_1,\mathbf{k}_1,\sigma_1;s_2,\mathbf{k}_2,\sigma_2}$, where s_1 and s_2 are the indices of Majorana operators (1 or 2). The expression is given by

$$
\begin{aligned}
h_{s_1,\mathbf{k_1}\sigma_1;s_2,\mathbf{k_2}\sigma_2}&=4\frac{\delta E}{\delta\gamma_{s_1,\mathbf{k}_1,\sigma_1;s_2,\mathbf{k}_2,\sigma_2}}\\
&=-\delta_{s_1,1}\delta_{s_2,1}\delta_{\sigma_1,\uparrow}\delta_{\sigma_2,\uparrow}\sum_{\mathbf{k}}(\gamma_{1,\mathbf{k},\downarrow;1,\mathbf{k}+\mathbf{k_1}-\mathbf{k_2},\downarrow}+\gamma_{2,\mathbf{k},\downarrow;2,\mathbf{k}+\mathbf{k_1}-\mathbf{k_2},\downarrow})
\end{aligned}
$$

$$
\begin{aligned}
&+ \delta_{s_1,1}\delta_{s_2,1}\delta_{\sigma_1,\uparrow}\delta_{\sigma_2,\downarrow}\sum_{\mathbf{k}}(\gamma_{2,\mathbf{k_1}+\mathbf{k_2}-\mathbf{k},\downarrow;2,\mathbf{k},\uparrow}-\gamma_{1,\mathbf{k_1}+\mathbf{k_2}-\mathbf{k},\downarrow;1,\mathbf{k},\uparrow}+\gamma_{1,\mathbf{k},\downarrow;1,\mathbf{k}+\mathbf{k_1}-\mathbf{k_2},\uparrow}+\gamma_{2,\mathbf{k},\downarrow;2,\mathbf{k}+\mathbf{k_1}-\mathbf{k_2},\uparrow})\\
&+ \delta_{s_1,1}\delta_{s_2,1}\delta_{\sigma_1,\downarrow}\delta_{\sigma_2,\uparrow}\sum_{\mathbf{k}}(-\gamma_{1,\mathbf{k},\uparrow;1,\mathbf{k_1}+\mathbf{k_2}-\mathbf{k},\downarrow}+\gamma_{2,\mathbf{k},\uparrow;2,\mathbf{k_1}+\mathbf{k_2}-\mathbf{k},\downarrow}+\gamma_{1,\mathbf{k},\uparrow;1,\mathbf{k}+\mathbf{k_1}-\mathbf{k_2},\downarrow}+\gamma_{2,\mathbf{k},\uparrow;2,\mathbf{k}+\mathbf{k_1}-\mathbf{k_2},\downarrow})\\
&- \delta_{s_1,1}\delta_{s_2,1}\delta_{\sigma_1,\downarrow}\delta_{\sigma_2,\downarrow}\sum_{\mathbf{k}}(\gamma_{1,\mathbf{k},\uparrow;1,\mathbf{k}+\mathbf{k_1}-\mathbf{k_2},\uparrow}+\gamma_{2,\mathbf{k},\uparrow;2,\mathbf{k}+\mathbf{k_1}-\mathbf{k_2},\uparrow})\\
&+ \delta_{s_1,1}\delta_{s_2,2}\delta_{\sigma_1,\uparrow}\delta_{\sigma_2,\uparrow}\left[\frac{U_{\mathrm{bf}}}{V}+\sum_{\mathbf{k}}\delta_{\mathbf{k_1},\mathbf{k_2}}\left(\varepsilon_f(\mathbf{k})-\mu_\sigma+\frac{U_{\mathrm{ff}}}{2}\right)+\sum_{\mathbf{k}}(\gamma_{1,\mathbf{k},\downarrow;2,\mathbf{k}+\mathbf{k_1}-\mathbf{k_2},\downarrow}-\gamma_{2,\mathbf{k},\downarrow;1,\mathbf{k}+\mathbf{k_1}-\mathbf{k_2},\downarrow})\right]\\
&+ \delta_{s_1,1}\delta_{s_2,2}\delta_{\sigma_1,\uparrow}\delta_{\sigma_2,\downarrow}\sum_{\mathbf{k}}(\gamma_{2,\mathbf{k},\downarrow;1,\mathbf{k}+\mathbf{k_1}-\mathbf{k_2},\uparrow}-\gamma_{1,\mathbf{k},\downarrow;2,\mathbf{k}+\mathbf{k_1}-\mathbf{k_2},\uparrow}-\gamma_{1,\mathbf{k_1}+\mathbf{k_2}-\mathbf{k},\downarrow;2,\mathbf{k},\uparrow}-\gamma_{2,\mathbf{k_1}+\mathbf{k_2}-\mathbf{k},\downarrow;1,\mathbf{k},\uparrow})\\
&+ \delta_{s_1,1}\delta_{s_2,2}\delta_{\sigma_1,\downarrow}\delta_{\sigma_2,\uparrow}\sum_{\mathbf{k}}(\gamma_{2,\mathbf{k},\uparrow;1,\mathbf{k}+\mathbf{k_1}-\mathbf{k_2},\downarrow}-\gamma_{1,\mathbf{k},\uparrow;2,\mathbf{k}+\mathbf{k_1}-\mathbf{k_2},\downarrow}-\gamma_{1,\mathbf{k},\uparrow;2,\mathbf{k_1}+\mathbf{k_2}-\mathbf{k},\downarrow}-\gamma_{2,\mathbf{k},\uparrow;1,\mathbf{k_1}+\mathbf{k_2}-\mathbf{k},\downarrow})\\
&+ \delta_{s_1,1}\delta_{s_2,2}\delta_{\sigma_1,\downarrow}\delta_{\sigma_2,\downarrow}\left[\sum_{\mathbf{k}}\delta_{\mathbf{k_1},\mathbf{k_2}}\left(\varepsilon_f(\mathbf{k})-\mu_\sigma+\frac{U_{\mathrm{ff}}}{2}\right)+\sum_{\mathbf{k}}(\gamma_{1,\mathbf{k},\uparrow;2,\mathbf{k}+\mathbf{k_1}-\mathbf{k_2},\uparrow}-\gamma_{2,\mathbf{k},\uparrow;1,\mathbf{k}+\mathbf{k_1}-\mathbf{k_2},\uparrow})\right]\\
&- \delta_{s_1,2}\delta_{s_2,1}\delta_{\sigma_1,\uparrow}\delta_{\sigma_2,\uparrow}\left[\frac{U_{\mathrm{bf}}}{V}+\sum_{\mathbf{k}}\delta_{\mathbf{k_1},\mathbf{k_2}}\left(\varepsilon_f(\mathbf{k})-\mu_\sigma+\frac{U_{\mathrm{ff}}}{2}\right)+\sum_{\mathbf{k}}(\gamma_{1,\mathbf{k},\downarrow;2,\mathbf{k}+\mathbf{k_1}-\mathbf{k_2},\downarrow}-\gamma_{2,\mathbf{k},\downarrow;1,\mathbf{k}+\mathbf{k_1}-\mathbf{k_2},\downarrow})\right]\\
&+ \delta_{s_1,2}\delta_{s_2,1}\delta_{\sigma_1,\uparrow}\delta_{\sigma_2,\downarrow}(\gamma_{1,\mathbf{k},\downarrow;2,\mathbf{k}+\mathbf{k_1}-\mathbf{k_2},\uparrow}-\gamma_{2,\mathbf{k},\downarrow;1,\mathbf{k}+\mathbf{k_1}-\mathbf{k_2},\uparrow}-\gamma_{1,\mathbf{k_1}+\mathbf{k_2}-\mathbf{k},\downarrow;2,\mathbf{k},\uparrow}-\gamma_{2,\mathbf{k_1}+\mathbf{k_2}-\mathbf{k},\downarrow;1,\mathbf{k},\uparrow})\\
&+ \delta_{s_1,2}\delta_{s_2,1}\delta_{\sigma_1,\downarrow}\delta_{\sigma_2,\uparrow}\sum_{\mathbf{k}}(\gamma_{1,\mathbf{k},\uparrow;2,\mathbf{k}+\mathbf{k_1}-\mathbf{k_2},\downarrow}-\gamma_{2,\mathbf{k},\uparrow;1,\mathbf{k}+\mathbf{k_1}-\mathbf{k_2},\downarrow}-\gamma_{1,\mathbf{k},\uparrow;2,\mathbf{k_1}+\mathbf{k_2}-\mathbf{k},\downarrow}-\gamma_{2,\mathbf{k},\uparrow;1,\mathbf{k_1}+\mathbf{k_2}-\mathbf{k},\downarrow})\\
&- \delta_{s_1,2}\delta_{s_2,1}\delta_{\sigma_1,\downarrow}\delta_{\sigma_2,\downarrow}\left[\sum_{\mathbf{k}}\delta_{\mathbf{k_1},\mathbf{k_2}}\left(\varepsilon_f(\mathbf{k})-\mu_\sigma+\frac{U_{\mathrm{ff}}}{2}\right)+\sum_{\mathbf{k}}(\gamma_{1,\mathbf{k},\uparrow;2,\mathbf{k}+\mathbf{k_1}-\mathbf{k_2},\uparrow}-\gamma_{2,\mathbf{k},\uparrow;1,\mathbf{k}+\mathbf{k_1}-\mathbf{k_2},\uparrow})\right]\\
&- \delta_{s_1,2}\delta_{s_2,2}\delta_{\sigma_1,\uparrow}\delta_{\sigma_2,\uparrow}\sum_{\mathbf{k}}(\gamma_{1,\mathbf{k},\downarrow;1,\mathbf{k}+\mathbf{k_1}-\mathbf{k_2},\downarrow}+\gamma_{2,\mathbf{k},\downarrow;2,\mathbf{k}+\mathbf{k_1}-\mathbf{k_2},\downarrow})\\
&+ \delta_{s_1,2}\delta_{s_2,2}\delta_{\sigma_1,\uparrow}\delta_{\sigma_2,\downarrow}\sum_{\mathbf{k}}(\gamma_{1,\mathbf{k_1}+\mathbf{k_2}-\mathbf{k},\downarrow;1,\mathbf{k},\uparrow}-\gamma_{2,\mathbf{k_1}+\mathbf{k_2}-\mathbf{k},\downarrow;2,\mathbf{k},\uparrow}+\gamma_{1,\mathbf{k},\downarrow;1,\mathbf{k}+\mathbf{k_1}-\mathbf{k_2},\uparrow}+\gamma_{2,\mathbf{k},\downarrow;2,\mathbf{k}+\mathbf{k_1}-\mathbf{k_2},\uparrow})\\
&+ \delta_{s_1,2}\delta_{s_2,2}\delta_{\sigma_1,\downarrow}\delta_{\sigma_2,\uparrow}\sum_{\mathbf{k}}(\gamma_{1,\mathbf{k},\uparrow;1,\mathbf{k_1}+\mathbf{k_2}-\mathbf{k},\downarrow}-\gamma_{2,\mathbf{k},\uparrow;2,\mathbf{k_1}+\mathbf{k_2}-\mathbf{k},\downarrow}+\gamma_{1,\mathbf{k},\uparrow;1,\mathbf{k}+\mathbf{k_1}-\mathbf{k_2},\downarrow}+\gamma_{2,\mathbf{k},\uparrow;2,\mathbf{k}+\mathbf{k_1}-\mathbf{k_2},\downarrow})\\
&- \delta_{s_1,2}\delta_{s_2,2}\delta_{\sigma_1,\downarrow}\delta_{\sigma_2,\downarrow}\sum_{\mathbf{k}}(\gamma_{1,\mathbf{k},\uparrow;1,\mathbf{k}+\mathbf{k_1}-\mathbf{k_2},\uparrow}+\gamma_{2,\mathbf{k},\uparrow;2,\mathbf{k}+\mathbf{k_1}-\mathbf{k_2},\uparrow})\\
&+ 2t_b\sum_{\boldsymbol{\delta}}\left[e^{-i\mathbf{K}\cdot\boldsymbol{\delta}}\left(-\frac{1}{2}\right)^{2N_s}s_f\mathrm{Pf}(\gamma_F)\sqrt{1-e^{i\alpha}}\gamma_F^{-1}\sqrt{1-e^{i\alpha}}\right].
\end{aligned}
\tag{B1}
$$

APPENDIX C: DOUBLE OCCUPANCY AND MOMENTUM DISTRIBUTION

The double occupancy of background fermions is defined as

$$
d=\frac{1}{V}\sum_{\mathbf{i}}\langle\Psi_{\mathrm{NGS}}|c^\dagger_{\mathbf{i}\uparrow}c^\dagger_{\mathbf{i}\downarrow}c_{\mathbf{i}\downarrow}c_{\mathbf{i}\uparrow}|\Psi_{\mathrm{NGS}}\rangle. \tag{C1}
$$

We use the non-Gaussian state $|\Psi_{\mathrm{NGS}}\rangle=U_{\mathrm{LLP}}(b^\dagger_{\mathbf{K}}\otimes U_{\mathrm{GS}})|0\rangle$ as the trial variation state; by considering only the $\mathbf{K}=0$ case we get

$$
\begin{aligned}
d&=\frac{1}{V}\sum_{\mathbf{i}}\langle\Psi_{\mathrm{NGS}}|c^\dagger_{\mathbf{i}\uparrow}c^\dagger_{\mathbf{i}\downarrow}c_{\mathbf{i}\downarrow}c_{\mathbf{i}\uparrow}|\Psi_{\mathrm{NGS}}\rangle=\frac{1}{V}\sum_{\mathbf{i}}\langle0|(U^\dagger_{\mathrm{GS}}b_{\mathbf{0}})U^\dagger_{\mathrm{LLP}}c^\dagger_{\mathbf{i}\uparrow}c^\dagger_{\mathbf{i}\downarrow}c_{\mathbf{i}\downarrow}c_{\mathbf{i}\uparrow}U_{\mathrm{LLP}}(b^\dagger_{\mathbf{0}}U_{\mathrm{GS}})|0\rangle\\
&=\frac{1}{V^3}\sum_{\mathbf{k_1},\mathbf{k_2},\mathbf{k_3},\mathbf{k_4}}\langle0|(U^\dagger_{\mathrm{GS}}b_{\mathbf{0}})U^\dagger_{\mathrm{LLP}}c^\dagger_{\mathbf{k_1},\uparrow}c^\dagger_{\mathbf{k_2},\downarrow}c_{\mathbf{k_3},\downarrow}c_{\mathbf{k_4},\uparrow}\left(\sum_{\mathbf{i}}e^{-i(\mathbf{k_1}+\mathbf{k_2}-\mathbf{k_3}-\mathbf{k_4})\cdot\mathbf{i}}\right)U_{\mathrm{LLP}}(b^\dagger_{\mathbf{0}}U_{\mathrm{GS}})|0\rangle
\end{aligned}
$$

$$= \frac{1}{V^2}\sum_{\mathbf{k},\mathbf{k}',\mathbf{q}} \langle 0|(U_{\rm GS}^\dagger b_{\mathbf{0}})U_{\rm LLP}^\dagger c_{\mathbf{k},\uparrow}^\dagger c_{\mathbf{q}-\mathbf{k},\downarrow}^\dagger c_{\mathbf{q}-\mathbf{k}',\downarrow} c_{\mathbf{k}',\uparrow} U_{\rm LLP}(b_{\mathbf{0}}^\dagger U_{\rm GS})|0\rangle$$

$$= \frac{1}{V^2}\sum_{\mathbf{k},\mathbf{k}',\mathbf{q}} \langle 0|(U_{\rm GS}^\dagger b_{\mathbf{0}})c_{\mathbf{k},\uparrow}^\dagger c_{\mathbf{q}-\mathbf{k},\downarrow}^\dagger c_{\mathbf{q}-\mathbf{k}',\downarrow} c_{\mathbf{k}',\uparrow}(b_{\mathbf{0}}^\dagger U_{\rm GS})|0\rangle. \tag{C2}$$

Since we also have $b_{\mathbf{0}} = \frac{1}{\sqrt{V}}\sum_l b_l$ and $b_{\mathbf{0}}^\dagger = \frac{1}{\sqrt{V}}\sum_l b_l^\dagger$, the equation becomes

$$d = \frac{1}{V^2}\sum_{\mathbf{k},\mathbf{k}',\mathbf{q}} \langle 0|(U_{\rm GS}^\dagger b_{\mathbf{0}})c_{\mathbf{k},\uparrow}^\dagger c_{\mathbf{q}-\mathbf{k},\downarrow}^\dagger c_{\mathbf{q}-\mathbf{k}',\downarrow} c_{\mathbf{k}',\uparrow}(b_{\mathbf{0}}^\dagger U_{\rm GS})|0\rangle$$

$$= \frac{1}{V^3}\sum_{\mathbf{k},\mathbf{k}',\mathbf{q}}\sum_{l_1,l_2} \langle 0|U_{\rm GS}^\dagger b_{l_1} c_{\mathbf{k},\uparrow}^\dagger c_{\mathbf{q}-\mathbf{k},\downarrow}^\dagger c_{\mathbf{q}-\mathbf{k}',\downarrow} c_{\mathbf{k}',\uparrow} b_{l_2}^\dagger U_{\rm GS}|0\rangle$$

$$= \frac{1}{V^2}\sum_{\mathbf{k},\mathbf{k}',\mathbf{q}} \langle 0|U_{\rm GS}^\dagger c_{\mathbf{k},\uparrow}^\dagger c_{\mathbf{q}-\mathbf{k},\downarrow}^\dagger c_{\mathbf{q}-\mathbf{k}',\downarrow} c_{\mathbf{k}',\uparrow} U_{\rm GS}|0\rangle. \tag{C3}$$

The next step is to rewrite this expression using Majorana operators and calculate the expectation value as

$$\begin{aligned}
d &= \frac{1}{V^2}\sum_{\mathbf{k},\mathbf{k}',\mathbf{q}} \langle c_{\mathbf{k},\uparrow}^\dagger c_{\mathbf{q}-\mathbf{k},\downarrow}^\dagger c_{\mathbf{q}-\mathbf{k}',\downarrow} c_{\mathbf{k}',\uparrow}\rangle_{\rm GS} \\
&= \frac{1}{16V^2}\sum_{\mathbf{k},\mathbf{k}',\mathbf{q}} \langle (a_{1\mathbf{k}}^\uparrow - ia_{2\mathbf{k}}^\uparrow)(a_{1\mathbf{q}-\mathbf{k}}^\downarrow - ia_{2\mathbf{q}-\mathbf{k}}^\downarrow)(a_{1\mathbf{q}-\mathbf{k}'}^\downarrow + ia_{2\mathbf{q}-\mathbf{k}'}^\downarrow)(a_{1\mathbf{k}'}^\uparrow + ia_{2\mathbf{k}'}^\uparrow)\rangle_{\rm GS} \\
&= \frac{1}{4} + \frac{1}{8V}\sum_{\mathbf{k}}(\gamma_{1,\mathbf{k},\uparrow;2,\mathbf{k},\uparrow} + \gamma_{1,\mathbf{k},\downarrow;2,\mathbf{k},\downarrow} - \gamma_{2,\mathbf{k},\downarrow;1,\mathbf{k},\downarrow} - \gamma_{2,\mathbf{k},\uparrow;1,\mathbf{k},\uparrow}) \\
&\quad + \frac{1}{16V^2}\sum_{\mathbf{k},\mathbf{k}',\mathbf{q}} [(\gamma_{1,\mathbf{k},\uparrow;1,\mathbf{q}-\mathbf{k},\downarrow} - \gamma_{2,\mathbf{k},\uparrow;2,\mathbf{q}-\mathbf{k},\downarrow})(\gamma_{2,\mathbf{q}-\mathbf{k}',\downarrow;2,\mathbf{k}',\uparrow} - \gamma_{1,\mathbf{q}-\mathbf{k}',\downarrow;1,\mathbf{k}',\uparrow}) \\
&\quad + (\gamma_{1,\mathbf{k},\uparrow;1,\mathbf{q}-\mathbf{k}',\downarrow} + \gamma_{2,\mathbf{k},\uparrow;2,\mathbf{q}-\mathbf{k}',\downarrow})(\gamma_{1,\mathbf{q}-\mathbf{k},\downarrow;1,\mathbf{k}',\uparrow} + \gamma_{2,\mathbf{q}-\mathbf{k},\downarrow;2,\mathbf{k}',\uparrow}) \\
&\quad - (\gamma_{1,\mathbf{k},\uparrow;1,\mathbf{k}',\uparrow} + \gamma_{2,\mathbf{k},\uparrow;2,\mathbf{k}',\uparrow})(\gamma_{1,\mathbf{q}-\mathbf{k},\downarrow;1,\mathbf{q}-\mathbf{k}',\downarrow} + \gamma_{2,\mathbf{q}-\mathbf{k},\downarrow;2,\mathbf{q}-\mathbf{k}',\downarrow}) \\
&\quad + (\gamma_{1,\mathbf{k},\uparrow;2,\mathbf{q}-\mathbf{k}',\downarrow} - \gamma_{2,\mathbf{k},\uparrow;1,\mathbf{q}-\mathbf{k}',\downarrow})(\gamma_{2,\mathbf{q}-\mathbf{k},\downarrow;1,\mathbf{k}',\uparrow} - \gamma_{1,\mathbf{q}-\mathbf{k},\downarrow;2,\mathbf{k}',\uparrow}) \\
&\quad - (\gamma_{1,\mathbf{k},\uparrow;2,\mathbf{q}-\mathbf{k},\downarrow} + \gamma_{2,\mathbf{k},\uparrow;1,\mathbf{q}-\mathbf{k},\downarrow})(\gamma_{1,\mathbf{q}-\mathbf{k}',\downarrow;2,\mathbf{k}',\uparrow} + \gamma_{2,\mathbf{q}-\mathbf{k}',\downarrow;1,\mathbf{k}',\uparrow}) \\
&\quad + (\gamma_{1,\mathbf{k},\uparrow;2,\mathbf{k}',\uparrow} - \gamma_{2,\mathbf{k},\uparrow;1,\mathbf{k}',\uparrow})(\gamma_{1,\mathbf{q}-\mathbf{k},\downarrow;2,\mathbf{q}-\mathbf{k}',\downarrow} - \gamma_{2,\mathbf{q}-\mathbf{k},\downarrow;1,\mathbf{q}-\mathbf{k}',\downarrow})].
\end{aligned} \tag{C4}$$

Similarly, we can obtain the expression for the background momentum distribution $n_\sigma(\mathbf{k})$ as

$$\begin{aligned}
n_\sigma(\mathbf{k}) = \langle c_{\mathbf{k}\sigma}^\dagger c_{\mathbf{k}\sigma}\rangle_{\rm GS} &= \tfrac{1}{4}\langle (a_{1,\mathbf{k}}^\sigma - ia_{2,\mathbf{k}}^\sigma)(a_{1,\mathbf{k}}^\sigma + ia_{2,\mathbf{k}}^\sigma)\rangle_{\rm GS} \\
&= \tfrac{1}{4}\langle 2 + ia_{1,\mathbf{k}}^\sigma a_{2,\mathbf{k}}^\sigma - ia_{2,\mathbf{k}}^\sigma a_{1,\mathbf{k}}^\sigma\rangle_{\rm GS} \\
&= \tfrac{1}{2} + \tfrac{1}{4}(\gamma_{1,\mathbf{k},\sigma;2,\mathbf{k},\sigma} - \gamma_{2,\mathbf{k},\sigma;1,\mathbf{k},\sigma}).
\end{aligned} \tag{C5}$$

[1] L. Landau and S. Pekar, Zh. Eksp. Teor. Fiz **18**, 419 (1948).
[2] A. Alexandrov and J. Devreese, *Advances in Polaron Physics* (Springer, Berlin, 2010).
[3] C. Franchini, M. Reticcioli, M. Setvin, and U. Diebold, Nat. Rev. Mater. **6**, 560 (2021).
[4] G. B. Partridge, W. Li, R. I. Kamar, Y. Liao, and R. G. Hulet, Science **311**, 503 (2006).
[5] M. W. Zwierlein, A. Schirotzek, C. H. Schunck, and W. Ketterle, Science **311**, 492 (2006).
[6] M. W. Zwierlein, C. H. Schunck, A. Schirotzek, and W. Ketterle, Nature (London) **442**, 54 (2006).
[7] M. Koschorreck, D. Pertot, E. Vogt, B. Fröhlich, M. Feld, and M. Köhl, Nature (London) **485**, 619 (2012).
[8] A. P. Chikkatur, A. Görlitz, D. M. Stamper-Kurn, S. Inouye, S. Gupta, and W. Ketterle, Phys. Rev. Lett. **85**, 483 (2000).
[9] J. Catani, G. Lamporesi, D. Naik, M. Gring, M. Inguscio, F. Minardi, A. Kantian, and T. Giamarchi, Phys. Rev. A **85**, 023623 (2012).
[10] N. Spethmann, F. Kindermann, S. John, C. Weber, D. Meschede, and A. Widera, Phys. Rev. Lett. **109**, 235301 (2012).
[11] N. B. Jørgensen, L. Wacker, K. T. Skalmstang, M. M. Parish, J. Levinsen, R. S. Christensen, G. M. Bruun, and J. J. Arlt, Phys. Rev. Lett. **117**, 055302 (2016).
[12] M.-G. Hu, M. J. Van de Graaff, D. Kedar, J. P. Corson, E. A. Cornell, and D. S. Jin, Phys. Rev. Lett. **117**, 055301 (2016).

[13] Z. Z. Yan, Y. Ni, C. Robens, and M. W. Zwierlein, Science **368**, 190 (2020).
[14] G. Ness, C. Shkedrov, Y. Florshaim, O. K. Diessel, J. von Milczewski, R. Schmidt, and Y. Sagi, Phys. Rev. X **10**, 041019 (2020).
[15] H. Tajima, J. Takahashi, S. I. Mistakidis, E. Nakano, and K. Iida, Atoms **9**, 18 (2021).
[16] F. Scazza, M. Zaccanti, P. Massignan, M. M. Parish, and J. Levinsen, Atoms **10**, 55 (2022).
[17] R. P. Feynman, Phys. Rev. **97**, 660 (1955).
[18] J. Tempere, W. Casteels, M. K. Oberthaler, S. Knoop, E. Timmermans, and J. T. Devreese, Phys. Rev. B **80**, 184504 (2009).
[19] S. P. Rath and R. Schmidt, Phys. Rev. A **88**, 053632 (2013).
[20] N.-E. Guenther, P. Massignan, M. Lewenstein, and G. M. Bruun, Phys. Rev. Lett. **120**, 050405 (2018).
[21] L. A. P. Ardila and S. Giorgini, Phys. Rev. A **92**, 033612 (2015).
[22] L. A. P. Ardila and S. Giorgini, Phys. Rev. A **94**, 063640 (2016).
[23] N. V. Prokof'ev and B. V. Svistunov, Phys. Rev. Lett. **81**, 2514 (1998).
[24] A. S. Mishchenko, N. V. Prokof'ev, A. Sakamoto, and B. V. Svistunov, Phys. Rev. B **62**, 6317 (2000).
[25] J. Vlietinck, J. Ryckebusch, and K. Van Houcke, Phys. Rev. B **89**, 085119 (2014).
[26] P. Kroiss and L. Pollet, Phys. Rev. B **90**, 104510 (2014).
[27] P. Massignan and G. M. Bruun, Eur. Phys. J. D **65**, 83 (2011).
[28] R. Combescot, A. Recati, C. Lobo, and F. Chevy, Phys. Rev. Lett. **98**, 180402 (2007).
[29] P. Massignan, Z. Yu, and G. M. Bruun, Phys. Rev. Lett. **110**, 230401 (2013).
[30] F. Grusdt, R. Schmidt, Y. E. Shchadilova, and E. Demler, Phys. Rev. A **96**, 013607 (2017).
[31] J. von Milczewski, F. Rose, and R. Schmidt, Phys. Rev. A **105**, 013317 (2022).
[32] F. Chevy, Phys. Rev. A **74**, 063628 (2006).
[33] T. Shi, E. Demler, and J. I. Cirac, Ann. Phys. (NY) **390**, 245 (2018).
[34] R. Liu, Y.-R. Shi, and W. Zhang, Phys. Rev. A **102**, 033305 (2020).
[35] P. Massignan, M. Zaccanti, and G. M. Bruun, Rep. Prog. Phys. **77**, 034401 (2014).
[36] W. Li and S. Das Sarma, Phys. Rev. A **90**, 013618 (2014).
[37] S. Ding, G. A. Domínguez-Castro, A. Julku, A. Camacho-Guardian, and G. M. Bruun, SciPost Phys. **14**, 143 (2023).
[38] Y. Shimazaki, C. Kuhlenkamp, I. Schwartz, T. Smoleński, K. Watanabe, T. Taniguchi, M. Kroner, R. Schmidt, M. Knap, and A. Imamoğlu, Phys. Rev. X **11**, 021027 (2021).
[39] V. E. Colussi, F. Caleffi, C. Menotti, and A. Recati, Phys. Rev. Lett. **130**, 173002 (2023).
[40] I. Amelio, N. D. Drummond, E. Demler, R. Schmidt, and A. Imamoglu, Phys. Rev. B **107**, 155303 (2023).
[41] Y. Nishida, Phys. Rev. Lett. **114**, 115302 (2015).
[42] W. Yi and X. Cui, Phys. Rev. A **92**, 013620 (2015).
[43] M. Pierce, X. Leyronas, and F. Chevy, Phys. Rev. Lett. **123**, 080403 (2019).
[44] H. Hu, J. Wang, J. Zhou, and X.-J. Liu, Phys. Rev. A **105**, 023317 (2022).
[45] M. Kutschera and W. Wójcik, Phys. Rev. C **47**, 1077 (1993).
[46] K. Fukushima and V. Skokov, Prog. Part. Nucl. Phys. **96**, 154 (2017).
[47] W. Zuo, Z. H. Li, G. C. Lu, J. Q. Li, W. Scheid, U. Lombardo, H. J. Schulze, and C. W. Shen, Phys. Lett. B **595**, 44 (2004).
[48] T. D. Lee, F. E. Low, and D. Pines, Phys. Rev. **90**, 297 (1953).
[49] A. Schirotzek, C.-H. Wu, A. Sommer, and M. W. Zwierlein, Phys. Rev. Lett. **102**, 230402 (2009).
[50] C. Kohstall, M. Zaccanti, M. Jag, A. Trenkwalder, P. Massignan, G. M. Bruun, F. Schreck, and R. Grimm, Nature (London) **485**, 615 (2012).
[51] T. Hartke, B. Oreg, C. Turnbaugh, N. Jia, and M. Zwierlein, Science **381**, 82 (2023).
[52] L. Hackl, T. Guaita, T. Shi, J. Haegeman, E. Demler, and I. Cirac, SciPost Phys. **9**, 048 (2020).
[53] E. Altman, E. Demler, and M. D. Lukin, Phys. Rev. A **70**, 013603 (2004).
[54] M. Greiner, C. A. Regal, J. T. Stewart, and D. S. Jin, Phys. Rev. Lett. **94**, 110401 (2005).
[55] C. V. Kraus, M. M. Wolf, J. I. Cirac, and G. Giedke, Phys. Rev. A **79**, 012306 (2009).
[56] Y. Nakano, M. M. Parish, and J. Levinsen, Phys. Rev. A **109**, 013325 (2024).
[57] L. A. P. Ardila, G. E. Astrakharchik, and S. Giorgini, Phys. Rev. Res. **2**, 023405 (2020).
[58] Y.-R. Shi, Y.-Y. He, R. Liu, and W. Zhang, New J. Phys. **25**, 093049 (2023).
[59] I. M. Georgescu, S. Ashhab, and F. Nori, Rev. Mod. Phys. **86**, 153 (2014).
[60] C. Gross and I. Bloch, Science **357**, 995 (2017).